The Effect of Biofilms on Turbulent Boundary Layers

M. P. Schultz
Research Engineer. Mem. ASME
e-mail: schultz@fit.edu

G. W. Swain
Professor.
e-mail: swain@fit.edu

Ocean Engineering Program,
Florida Institute of Technology,
150 West University Blvd.,
Melbourne, FL 32901

Materials exposed in the marine environment, including those protected by antifouling paints, may rapidly become colonized by microfouling. This may affect frictional resistance and turbulent boundary layer structure. This study compares the mean and turbulent boundary layer velocity characteristics of surfaces covered with a marine biofilm with those of a smooth surface. Measurements were made in a nominally zero pressure gradient, boundary layer flow with a two-component laser Doppler velocimeter at momentum thickness Reynolds numbers of 5600 to 19,000 in a recirculating water tunnel. Profiles of the mean and turbulence velocity components, including the Reynolds shear stress, were measured. An average increase in the skin friction coefficient of 33 to 187 percent was measured on the fouled specimens. The skin friction coefficient was found to be dependent on both biofilm thickness and morphology. The biofilms tested showed varying effect on the Reynolds stresses when those quantities were normalized with the friction velocity.

Introduction

While modern antifouling (AF) systems are effective in controlling most macrofouling (e.g., barnacles, tubeworms, macroalgae, etc.), they do become colonized by microfouling organisms that produce a slime film. In some cases, the growth of this film is stimulated on copper and organo-tin AF paints (Loeb et al., 1984). The effect of biofilms on frictional resistance and turbulent boundary structure is, therefore, of great interest in predicting the hydrodynamic performance of marine vehicles.

A significant body of research has been devoted to studying the effects of marine fouling on frictional resistance. Much of the early work is documented in *Marine Fouling and Its Prevention* (1952). Most of this research addressed the effects of macrofouling. The first anecdotal evidence that slime films increase skin friction was given by Sir Archibald Denny in his discussion of a paper by McEntee (1915). Denny stated that microbial fouling on full-scale ships increased the resistance at a rate of $\frac{1}{2}$ percent per day while at dock. Researchers at Langley Field, in experiments on towed plates, demonstrated that slime films significantly increase skin friction (Benson et al., 1938). An extensive investigation into the effects of microbial slime layers on pipe flow was carried out by Picologlou et al. (1980). They noted that the thickness and morphology of the slime film is affected by the hydrodynamic conditions to which it is exposed. It was also observed that the viscoelastic character of the biofilm combined with its filamentous nature seemed to cause additional energy dissipation mechanisms that led to higher frictional resistance.

Lewkowicz and Das (1981) used uniformly distributed nylon tufts attached to a rough flat plate in order to model a marine slime growth. Detailed profiles of both mean and turbulence quantities were measured. They found that the skin friction in a zero pressure gradient flow was an average of 18 percent higher for the model slime film with a background roughness than for the background roughness alone. Loeb et al. (1984) measured the influence of microbial biofilms on the hydrodynamic drag of rotating discs. Their data showed an increase in frictional resistance of 10 to 20 percent due to slime films. Preroughened disks were also tested both before and after exposure to biofilm formation, since it was hypothesized that a thin slime film might reduce the drag of rough surfaces by effectively smoothing them. This was not the case, as an increase in frictional drag of 10 percent was measured for the fouled, rough disk.

Lewthwaite et al. (1985) conducted an experiment in which velocity profiles were taken on a vessel at sea over a two year period. In this study, a 23 m fleet tender was operated in temperate waters and was subjected to marine biofouling buildup. A pitot-static tube traverse system was outfitted on the ship by means of several through-hull fittings located along the length of the hull. The local skin friction coefficient was found from the mean velocity profile. They measured an increase in c_f from 0.0023 to 0.0042 over the exposure period. A corresponding 15 percent reduction in ship speed was observed. There were no quantitative measurements made on the fouling settlement on the hull. However, it was noted that when the vessel was drydocked, it was virtually free of hard fouling and macroalgae. It was covered with a dense slime film estimated to be 1 mm thick. When the hull was cleaned and returned to the water, measurements confirmed that c_f returned approximately to its clean hull value.

Haslbeck and Bohlander (1992) conducted a full-scale ship trial in order to quantify the effect of microbial biofilms on ship drag. In their investigation, the *USS Brewton,* a Knox class frigate, was instrumented to measure shaft horsepower and ship speed over a mile course. The ship, which was coated with an ablative antifouling paint containing both cuprous oxide and tributyltin oxide, had been subjected to fouling in Pearl Harbor, Hawaii for 22 months. An initial hull inspection by divers indicated the presence of a microbial biofilm but little hard fouling. It was found that there was as much as an 18 percent decrease in the required shaft horsepower to propel the ship at same speed after the microbial biofilm was removed.

While it has been shown that biofilms have the potential to increase ship drag, the authors are unaware of any previous study in which the mean and turbulence structure of boundary layer flows over natural marine biofilms were measured. This information is vital to the understanding and prediction of flows over fouled hulls.

Experimental Facilities and Method

The experimental work was carried out at the Harbor Branch Oceanographic Institution (HBOI) water tunnel (Gangadharan et al., 1996). The tunnel is 2.44 m in height, 8.53 m in length, and 1.22 m in width and is constructed of mild steel coated

Contributed by the Fluids Engineering Division for publication in the JOURNAL OF FLUIDS ENGINEERING. Manuscript received by the Fluids Engineering Division August 17, 1998; revised manuscript received December 8, 1998. Associate Technical Editor: P. Bradshaw.

 Copyright © 1999 by ASME

Downloaded 01 Apr 2008 to 131.122.81.5. Redistribution subject to ASME license or copyright; see http://www.asme.org/terms/Terms_Use.cfm

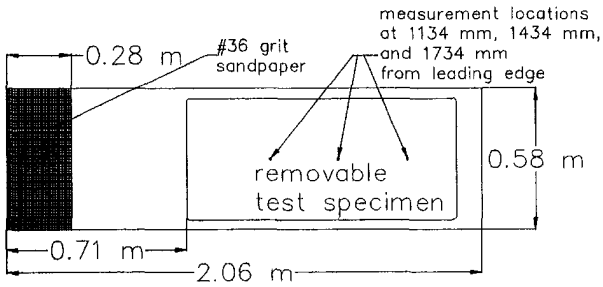

Fig. 1 Boundary layer test fixture

with marine polyamide epoxy. The test section is 0.61 m by 0.61 m and is 2.54 m in length. The contraction ratio in the tunnel is 4 to 1. Flow management devices include turning vanes placed in the tunnel corners and a polycarbonate honeycomb flow straightener in the entrance to the contraction section. The resulting freestream turbulence intensity in the test section ranged from 2.5 to 3.0 percent in the velocity range that was used in the present experiment. The freestream velocities in the test section can be adjusted from 1.2 m/s to 4.0 m/s.

The test matrix consisted of five specimens. Two smooth, unfouled surfaces were used as controls. The remaining three specimens were subjected to biofilm build-up for 6, 14, and 17 days. In order to look at boundary layer development and the effect of varying Reynolds number, velocity profiles were taken at three downstream positions. The profiles were taken at 1.13 m, 1.43 m, and 1.73 m from the leading edge and at three freestream velocities (nominally 1.5 m/s, 2.25 m/s, and 3.0 m/s). Velocity profiles consisted of about 50 logarithmically spaced sampling locations across the boundary layer.

The test specimens were inserted into a flat plate mounted horizontally in the tunnel (Fig. 1). The plate was 0.58 m in width, 2.06 m in length, and 54 mm thick. It was constructed of polyvinylchloride (PVC) and stainless steel and was mounted horizontally in the tunnel's test section. The leading edge of the test plate was shaped to mimic the forward portion of a NACA 0012-64 airfoil. The forward most 280 mm of plate was covered with #36 grit sandpaper to hasten development of a turbulent boundary layer. The use of a strip of roughness to artificially thicken a boundary layer was proposed by Klebanoff and Diehl (1951). The test specimens were fabricated from a cast acrylic sheet. Each specimen measured 558 mm in width, 1168 mm in length, and 12.7 mm in thickness. The forward edge of the specimen was located 710 mm from the leading edge of the plate.

Velocity measurements were made using a TSI two-component, fiber-optic laser Doppler velocimeter (LDV) system. The LDV probe was mounted on an AMPRO System 1618, three-axis traverse unit. The traverse allowed the position of the probe to be maintained to ± 5 μm in all directions. In order to facilitate two-component, near wall measurements, the probe was tilted downwards at an angle of 4 deg to the horizontal and was rotated 45 deg about its axis. This minimized bias error due to introduction of the w' fluctuations into the v' measurements. Using this setup, measurements as close as 40 μm to the wall were made. Velocity measurements were conducted in coincidence mode with 10,000 random samples per location. Doppler bursts for the two channels were required to fall within a set coincidence window or the sample was rejected. This coincidence window was set at 50 μs, 30 μs, and 20 μs for the 1.5 m/s, 2.25 m/s, and 3.0 m/s flows, respectively.

The biofilms on the fouled test specimens were grown at the HBOI Aquaculture facility. Water from the Indian River Lagoon was continuously pumped through a sand filtration system and into three growout tanks. During these experiments, the salinity of the water in the tanks ranged from 20 ppt to 36 ppt. The water temperature ranged from 25°C to 35°C. The thickness of the biofilm on the test specimens was determined using a Gardco comb-type wet film paint thickness (WFT) gauge. It had a thickness measurement range of 25 μm to 2032 μm with a resolution of 25 μm in the 25 μm to 305 μm range. Sixty thickness measurements were made both before and after subjecting each biofilm to hydrodynamic testing in the water tunnel. These were made on the damp biofilm in air. After hydrodynamic testing, a sample of the biofilm was taken and examined under a compound microscope to identify the organisms present. A more detailed description of the experimental setup is provided in Schultz (1998).

In the present investigation, three methods were used to determine c_f for the smooth walls and two methods were used for the fouled walls. For the smooth specimens, c_f was determined using Bradshaw's method. The sublayer slope method and the Reynolds stress method were also used to verify these results. The details of Bradshaw's method, which is based on inner layer similarity, are given in Bradshaw (1959) and Winter (1977). Log-law reference values of $y^+ = 100$ and $U^+ = 16.24$ ($\kappa = 0.41, B = 5.0$) were used in the present study. The sublayer slope method uses the velocity gradient in the linear sublayer to obtain the wall shear stress. Data at $y^+ < 7$ were used. The final method that was used to find c_f on the smooth specimens was the Reynolds stress method, which is detailed by Lee et al. (1993). For the fouled plates, the analysis was a bit more complex. First, before c_f could be found, the location of the

Nomenclature

B = log-law intercept
C_F = frictional resistance coefficient = $(2F_D)/(\rho U_e^2 S)$
c_f = skin friction coefficient = $(2\tau_0)/(\rho U_e^2)$
F_D = drag force
H = shape factor = δ^*/θ
k = some measure of roughness height
k_s = equivalent sand roughness height
Re_x = Reynolds number based on x = xU_e/ν
Re_{δ^*} = displacement thickness Reynolds number = $\delta^* U_e/\nu$
Re_θ = momentum thickness Reynolds number = $\theta U_e/\nu$
S = wetted surface area
t = t-statistic
U, V = mean velocity in the x and y direction
U_e = freestream velocity
ΔU^+ = roughness function
u, v = instantaneous velocity in the x and y direction
u', v' = fluctuating velocity component in the x and y direction
U_τ = friction velocity = $\sqrt{\tau_o/\rho}$
x = streamwise distance from plate leading edge
y = normal distance from the boundary
α = statistical significance level
Δ = Clauser length scale = $\delta^* U_e/U_\tau$
δ = boundary layer thickness (y at $U = 0.99U_e$)
δ^* = displacement thickness
ϵ = wall datum error
κ = von Karman constant (=0.41)
ν = kinematic viscosity of the fluid
θ = momentum thickness
ρ = density of the fluid
τ_o = wall shear stress

Superscript

$+$ = inner variable (normalized with U_τ or U_τ/ν)

Downloaded 01 Apr 2008 to 131.122.81.5. Redistribution subject to ASME license or copyright; see http://www.asme.org/terms/Terms_Use.cfm

virtual origin ($y + \epsilon = 0$) had to be determined. This was accomplished using an adaptation of the method proposed by Perry and Joubert (1963). The log-law slope method, which is detailed in Lewthwaite et al. (1985) and the Reynolds stress method were then used to determine c_f.

Uncertainty Estimates

The precision uncertainties for the velocity measurements were determined using repeatability tests. Ten replicate profiles were taken on both a smooth and a fouled plate. The standard deviation for each of the measurement quantities was then calculated for both samples. In order to estimate the 95 percent confidence limits for a statistic calculated from a single profile, the standard deviation was multiplied by the two-tailed t value ($t = 2.262$) for 9 degrees of freedom and $\alpha = 0.05$, as given by Coleman and Steele (1995). The resulting precision uncertainties in the mean velocities were ± 1.0 percent in the outer region of the boundary layer and ± 1.9 percent in the near-wall region. For $\overline{u'^2}$ and $\overline{v'^2}$, the precision was ± 1.7 percent in the outer region and ± 3.4 percent in the near-wall region. The bias errors for the mean velocities were less than 2 percent. A bias error in the v' measurements of ~ 2 percent was caused by introduction of the w' component due to inclination of the LDV probe. The uncertainties in c_f for the smooth walls using Bradshaw's method, the sublayer slope method, and the Reynolds stress method were ± 5, ± 7, and ± 15 percent, respectively. The uncertainty in c_f for the rough walls using the log-law slope method was ± 15 percent and was ± 28 percent using the Reynolds stress method. The increased uncertainty resulted mainly from the extra two degrees of freedom (ϵ and ΔU^+) in the analysis of rough walls. The uncertainty in δ was ± 12 percent and resulted from the relatively high freestream turbulence and fluctuations in the freestream velocity. In order to test the significance of the differences in the boundary layer parameters that were observed, several analyses of variance (ANOVA) were used (Sokal and Rohfl, 1981).

Results and Discussion

In order to reference each of the test samples, an alphanumeric code is used. The first letter represents the test specimen type. "S" is a smooth plate. "F" is fouled plate. The first number indicates the replicate number. F1, F2, and F3 were exposed for 6, 14, and 17 days, respectively. To further facilitate the reference of individual velocity profiles, an additional letter and number are added to the previous designation. To indicate the downstream distance from the leading edge, x, the letters A–C are used. "A" represents the 1.13 m profiling station, "B" the 1.43 m station, and "C" the 1.73 m station. The nominal freestream velocity is indicated with the numbers 1–3. The number "1" represents 1.5 m/s, "2" represents 2.25 m/s, and "3" represents 3.0 m/s. For example, "S2B3" refers to a profile made on smooth specimen replicate 2 at $x = 1.43$ m and $U_e = 3.0$ m/s.

The biofilm on each of the three fouled plates was characterized by visual assessment both before and after hydrodynamic testing. The results of this evaluation are shown in Table 1. Examination of the biofilm with the aid of a microscope showed that the film on F1 was composed mainly of extracellular polymer substances (EPS), blue-green algae (*Anabaina oscillarioides*), and marine diatoms (dominated by *Melosira spp.*). F2 was fouled with EPS, green algae (*Enteromorpha spp.*), and marine diatoms (dominated by *Melosira spp.* and *Thallasiothrix spp.*). The biofilm on F3 was almost entirely composed of filamentous green algae (*Enteromorpha spp.*). The overall mean thickness (± 1 SD) of the biofilms based on 60 individual measurements was found. Before hydrodynamic testing, the thicknesses of F1, F2, and F3 were 350 μm $\pm$ 69 μm, 160 μm $\pm$ 41 μm, and 310 μm $\pm$ 100 μm, respectively. After hydrodynamic testing, the thicknesses of F1, F2, and F3 were 74 μm $\pm$ 46 μm, 130 μm $\pm$ 27 μm, and 340 μm $\pm$ 150 μm, respectively. The reduction in biofilm thickness for F1 and F2 after testing was due in large part to the removal of some portion of these films as a result of the wall shear stress. The thickness of F3 remained the same within measurement uncertainty.

Table 1 Visual assessment of fouled test specimens

Specimen	Total % Fouling Cover	Constituents and Their % Cover
F1 before	97	Slime 97% (light to medium density film)
F1 after	70	Slime 70% (very light density film)
F2 before	98	Slime 94% (medium density film) Filamentous green algae 4%
F2 after	91	Slime 90% (medium density film) Filamentous green algae 1%
F3 before	95	Slime 70% (medium density film) Filamentous green algae 25%
F3 after	82	Slime 70% (medium density film) Filamentous green algae 12%

Figure 2 shows the law of the wall profiles for S1 and the fouled specimens as they develop down the plate. The roughness function, ΔU^+, varied greatly with specimen as well as the downstream position. The profiles for F3, the biofilm dominated by filamentous green algae, generally had the largest roughness function. Biofilms F1 and F2, which consisted of a slime film, had less effect on the mean profile.

The basic boundary layer parameters calculated for the smooth and fouled test plates are shown in Table 2. The boundary layer thickness, δ, is specified for $U = 0.99U_e$. To determine if the differences were significant within the experimental uncertainty, statistical tests were conducted. These consisted of

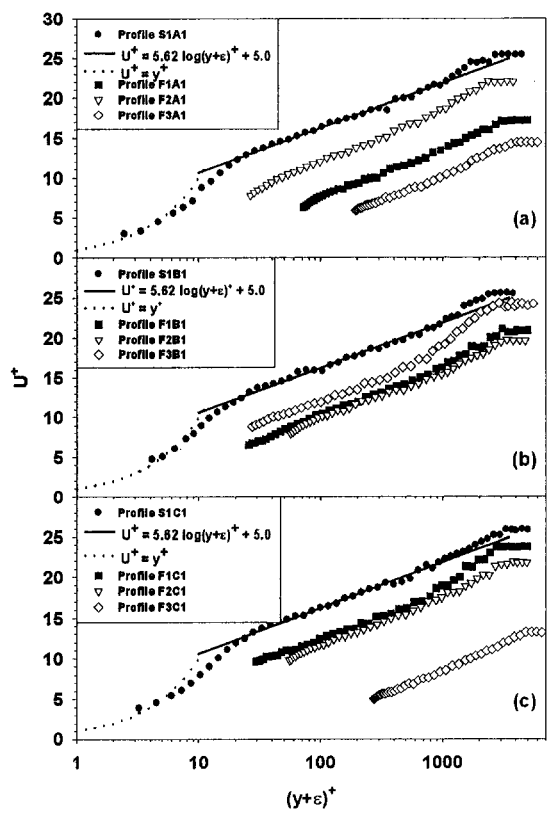

Fig. 2 Law of the wall plots for smooth and fouled specimens: (*a*) x = 1.13 m; (*b*) x = 1.43 m; (*c*) x = 1.73 m (uncertainties in U^+: ± 4 percent for smooth profiles; ± 11 percent for fouled profiles)

Downloaded 01 Apr 2008 to 131.122.81.5. Redistribution subject to ASME license or copyright; see http://www.asme.org/terms/Terms_Use.cfm

Table 2 Boundary layer parameters

Profile	Re_θ	δ (mm)	δ* (mm)	θ (mm)	Δ (mm)	H
S1A1	6500	33	4.3	3.4	110	1.29
S1B1	6500	33	4.4	3.4	110	1.31
S1C1	8100	43	5.4	4.2	140	1.28
S1A2	8500	33	3.8	3.0	100	1.29
S1B2	13000	38	4.6	3.6	120	1.27
S1C2	10000	36	4.6	3.6	120	1.28
S1A3	11000	32	3.8	2.9	100	1.30
S1B3	12000	33	3.9	3.1	100	1.25
S1C3	14000	43	5.0	4.0	130	1.25
S2A1	5600	30	3.9	3.0	100	1.29
S2B1	6300	35	4.3	3.4	110	1.28
S2C1	7000	37	4.7	3.6	120	1.32
S2A2	8500	28	3.8	3.0	100	1.29
S2B2	10000	35	4.4	3.5	120	1.27
S2C2	9000	37	4.3	3.4	110	1.26
S2A3	12000	30	3.9	3.0	110	1.29
S2B3	13000	36	4.4	3.5	120	1.25
S2C3	15000	36	4.3	3.4	120	1.25
F1A1	6500	29	5.0	3.6	86	1.41
F1B1	7600	37	6.0	4.1	130	1.44
F1C1	9200	38	6.87	5.0	160	1.37
F1A2	9730	30	4.81	3.5	82	1.39
F1B2	10000	35	5.07	3.6	88	1.41
F1C2	12000	37	6.0	4.2	120	1.42
F1A3	14000	39	4.9	3.8	110	1.28
F1B3	13000	32	4.4	3.4	110	1.30
F1C3	15000	37	5.4	4.1	140	1.31
F2A1	5700	27	4.3	3.1	95	1.40
F2B1	7500	35	5.5	4.0	110	1.36
F2C1	8200	40	6.0	4.5	130	1.33
F2A2	9500	30	4.7	3.5	110	1.34
F2B2	11000	34	5.5	4.0	140	1.35
F2C2	12000	39	5.9	4.5	150	1.31
F2A3	9800	26	3.7	2.7	83	1.37
F2B3	15000	36	5.5	4.3	140	1.30
F2C3	13000	35	4.9	3.7	100	1.31
F3A1	6700	28	5.6	3.8	80	1.49
F3B1	7700	35	6.5	4.4	160	1.48
F3C1	9400	38	8.1	5.4	109	1.49
F3A2	10000	34	5.6	3.9	69	1.44
F3B2	12000	35	6.3	4.5	160	1.41
F3C2	14000	43	7.6	5.1	95	1.48
F3A3	14000	33	5.4	3.9	76	1.39
F3B3	19000	38	7.0	5.2	170	1.36
F3C3	19000	38	7.6	5.3	140	1.42

two-way ANOVAs with specimen and Re_x as factors. In cases where the ANOVA indicated significant differences for one of the factors, multiple pairwise comparisons were run using Tukey's test (Sokal and Rohfl, 1981). The significance level for all the tests was set at $\alpha = 0.05$.

The ANOVA on the boundary layer thickness results showed that neither specimen nor Re_x had a significant effect. This may have been due to the high degree of variability in δ. For example, the absolute deviation of δ between the smooth plate replicates ranged from 2.0 to 13 percent of the mean for the 9 profiles and averaged 7.1 percent. This was due in part to the inability to control U_e more precisely in the water tunnel. Thole and Boggart (1996) have also observed that high freestream turbulence levels increase the uncertainty in finding δ. Results from Lewkowicz and Das (1981), on a simulated biofilm roughness, showed that biofilms had a thickening effect on the boundary layer of 25 to 30 percent above that of a background roughness.

Table 3 Skin friction coefficients for the smooth profiles

Profile	Re_θ	c_f (x10^3) Bradshaw Cross Plot	c_f (x10^3) Sublayer Slope	c_f (x10^3) Reynolds Stress
S1A1	6500	3.1	3.0	2.8
S1B1	6500	3.1	2.8	2.9
S1C1	8100	3.0	2.8	2.6
S1A2	8500	2.9	2.9	2.8
S1B2	13000	2.9	2.8	2.5
S1C2	10000	2.9	2.7	2.5
S1A3	11000	2.7	2.7	3.0
S1B3	12000	2.8	-	2.9
S1C3	14000	2.8	2.8	2.6
S2A1	5600	3.2	3.2	2.8
S2B1	6300	3.1	3.1	2.9
S2C1	7000	3.0	3.1	2.7
S2A2	8500	2.8	2.8	2.9
S2B2	10000	2.9	2.7	2.7
S2C2	9000	3.0	3.0	2.7
S2A3	12000	2.7	2.7	2.9
S2B3	13000	2.7	2.6	2.9
S2C3	15000	2.8	-	2.9

- missing data

The presence of the biofilm did have a significant effect on the boundary layer displacement thickness, δ^*. The ANOVA indicated an effect of specimen as well as Re_x. Multiple pairwise comparisons indicated a significant increase in δ^* over that of the smooth specimens for all the fouled specimens tested. Differences between all specimens were found with the exception of S1 versus S2 (the controls) and F1 versus F2. The shape factor, H, was significantly increased for the fouled profiles as well. Multiple pairwise comparisons showed differences for all the specimens with the exception of S1 versus S2 and F1 versus F2. The average increase in H with fouling was 7.0 percent for F1, 4.8 percent for F2, and 13 percent for F3 compared to the smooth plates. The increase in H with the presence of fouling was also seen by Lewkowicz and Das (1981) in flow over a model biofilm and is a typical surface roughness effect. The Clauser length, Δ, was not significantly affected by the presence of the biofilm. There was a higher degree of variability for the fouled specimens, however. It seems that this was related to the fouling extent, as F3, the most heavily fouled specimen, had the largest variability.

The skin friction coefficients for the smooth specimens are shown in Table 3 and Fig. 3. Agreement was found between the replicate smooth plate skin friction results within the uncertainty of the measurements (S1 and S2). There was also agreement between the values obtained using Bradshaw's method, the sublayer slope method, and the Reynolds stress method. Bradshaw's method was chosen to calculate the values of U_τ used in the profile plots. This was because a paucity of linear

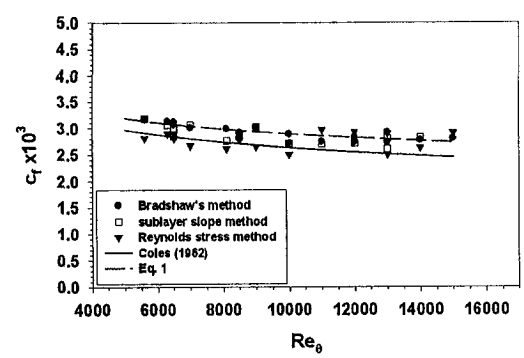

Fig. 3 Skin friction coefficients for the smooth plate profiles (uncertainties in c_f: ±5 percent for Bradshaw's method; ±7 percent for sublayer slope method; ±15 percent for Reynolds stress method)

Downloaded 01 Apr 2008 to 131.122.81.5. Redistribution subject to ASME license or copyright; see http://www.asme.org/terms/Terms_Use.cfm

Table 4 Skin friction coefficients for the fouled specimens

Profile	Re_θ	c_f (x10^3) Log-law Slope	c_f (x10^3) Reynolds Stress
F1A1	6500	6.8	4.7
F1B1	7600	4.5	6.4
F1C1	9200	3.5	4.3
F1A2	9730	7.0	4.4
F1B2	10000	6.7	4.4
F1C2	12000	4.7	4.2
F1A3	14000	4.2	4.0
F1B3	13000	3.3	3.5
F1C3	15000	2.9	3.8
F2A1	5700	4.1	4.3
F2B1	7500	5.2	4.5
F2C1	8200	4.2	3.6
F2A2	9500	3.5	4.8
F2B2	11000	3.0	4.8
F2C2	12000	2.9	3.5
F2A3	9800	4.0	4.6
F2B3	15000	3.1	4.0
F2C3	13000	4.7	4.4
F3A1	6700	9.7	8.0
F3B1	7700	3.4	5.2
F3C1	9400	11	10
F3A2	10000	13	5.8
F3B2	12000	3.1	5.2
F3C2	14000	13	8.6
F3A3	14000	10	5.8
F3B3	19000	3.6	5.5
F3C3	19000	6.0	7.8

sublayer data points led to a higher uncertainty in U_τ obtained using the sublayer slope method. It is of note that c_f for the smooth wall case averaged 6–9 percent higher than those given by Coles (1962) (see Fig. 3). This is probably an effect of the high freestream turbulence level. The following is the best-fit, power law of the present smooth plate results using Bradshaw's method:

$$c_f = \frac{0.0105}{\mathrm{Re}_\theta^{0.14}} \tag{1}$$

All the fouled plates had increased c_f values compared to the smooth condition. Fouled specimens F1, F2, and F3 showed increases in c_f of 8 to 130, 3 to 70, and 11 to 370 percent, respectively. The average increase was 70 percent for F1, 30 percent for F2, and 190 percent for F3. However, it should be mentioned that the high freestream turbulence may not affect the smooth and fouled wall c_f values in the same way.

The variation in c_f was greatly increased for the fouled plates. For example, S1 had a mean c_f ($\times 10^3$) (± 1 SD) of 2.9 $\pm$ 0.1, and S2 had a mean c_f ($\times 10^3$) of 2.9 $\pm$ 0.2. Fouled plates F1, F2, and F3 had mean c_f ($\times 10^3$) values of 4.8 $\pm$ 1.6, 3.9 $\pm$ 0.8, and 8.1 $\pm$ 4.2, respectively. A Kruskal-Wallis ANOVA on ranks and Student-Newman-Keuls pairwise comparisons (Sokal and Rohfl, 1981) indicated a significant difference between all of the smooth panels and the fouled panels with the exception of S1 versus S2 (the controls) and F1 versus F2. The c_f results for the fouled specimens show that not only biofilm thickness but also composition and morphology are important determining factors. The average increase in c_f for slime films with a mean thickness before testing of 160 μm and 350 μm was 33 and 68 percent, respectively. The increase in c_f for a surface dominated by filamentous green algae (*Enteromorpha spp.*) with a mean thickness of 310 μm averaged 190 percent. It seems, therefore, that the flapping motions of filamentous algae remove larger amounts of momentum from the mean flow than nonfilamentous films of the same thickness.

The results for the fouled plates indicate an increase in c_f for all the fouled plate profiles (Table 4 and Fig. 4). Both methods indicated increases for the fouled plates, although each method

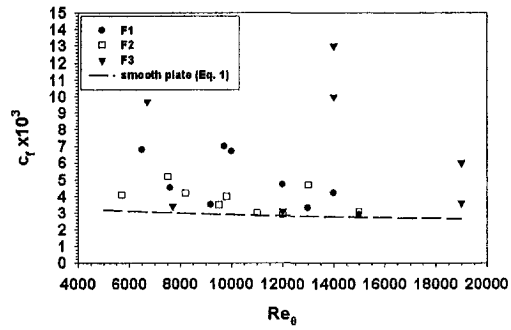

Fig. 4 Skin friction coefficients for the fouled plate profiles using the log-law slope method (uncertainty in c_f $\pm$ 15 percent)

showed high variability. The log-law slope method was used to calculate the values of U_τ used in the fouled plate profile plots because of the smaller uncertainty in this value relative to those obtained using the Reynolds stress method. In order to analyze the change in c_f for the fouled specimens, a comparison with the smooth plate results (Eq. (1)) at the same Re_θ was made.

Much of the variability within c_f results on the same specimen can be attributed to the complex and dynamic nature of the biofilm. First, it is heterogeneous in composition, structure, and distribution. This was especially true for F3. Biofilms may be thought of as a constantly varying streamwise roughness, not only in height but also in morphology. This brings the underlying assumption of boundary layer equilibrium, which is inherent to wall similarity methods, into question. A study by Andreopoulos and Wood (1982), in flows subjected to a short length of surface roughness, has found that boundary layers do not fully recover to a self-preserving state until downstream distances $>55\delta$. Work by Antonia and Luxton (1972) has shown, that on k-type surface roughness, the boundary layer adjusts rather slowly to a step change from rough to smooth surface condition. Antonia and Luxton (1971) have also observed that flows moving from smooth to rough surfaces adjust much more rapidly ($\sim 10\delta$). Further complicating the present situation was that some of the biofilm was removed over the course of the experiment due to the shear stress.

Some of the variation in the c_f results for the fouled plates may also be attributed to the method itself. Using Bradshaw's method for smooth plate flows, there is only a single free parameter, c_f. Additional parameters, ΔU^+ and ϵ, enter the analysis for rough wall flows. While the extra two degrees of freedom can produce a "better" log-law fit in a statistical sense, they can also lead to increased error in c_f. Natural scatter in the inner region data due to the influence of roughness elements may be masked in producing a least-squares fit of the log-law. Archarya and Escudier (1983) report that the use of rough wall analyses with ΔU^+ and ϵ not identically set to zero on smooth wall data produced c_f's with an average error of 12 percent.

Research by Perry et al. (1969), Ligrani and Moffat (1986), Bandyopadhyay (1987), and others has furthered the understanding of boundary layer flows over k-type and d-type roughnesses. Even in these "regular" roughness arrangements, the determination of c_f can be problematic. In general, an independent method for finding c_f is desirable. But, the common methods used on "regular" roughnesses, such as a floating element force balance or pressure taps, are not generally feasible on biofilms and could not be used in the present investigation.

Granville's (1987) method of finding the roughness function, ΔU^+, at the same value of Re_{δ^*} resulted in ΔU^+ ranging from 1.0 to 9.6, 0.54 to 6.5, and 1.8 to 15 for F1, F2, and F3, respectively (see Table 5). F1 had 33 percent of its profiles with k_s^+ values greater than 70, the value given by Schlichting (1979) as the onset of fully rough flow. F2 had no profiles

Downloaded 01 Apr 2008 to 131.122.81.5. Redistribution subject to ASME license or copyright; see http://www.asme.org/terms/Terms_Use.cfm

Table 5 Roughness parameters for the fouled profiles († overall mean biofilm after hydrodynamics testing)

Profile	ΔU^+	k_s^+	k_s (mm)	k (mm)	ε (mm)
F1A1	8.5	140	1.3	0.35	0.68
F1B1	5.0	33	0.38	0.35	0.30
F1C1	2.5	12	0.15	0.35	0.39
F1A2	9.6	220	1.3	0.35	0.53
F1B2	9.4	200	1.2	0.35	0.52
F1C2	6.4	58	0.42	0.35	0.43
F1A3	5.2	35	0.21	0.074†	0.23
F1B3	2.2	10	0.071	0.074†	0.31
F1C3	1.0	6.3	0.046	0.074†	0.32
F2A1	3.3	16	0.19	0.16	0.32
F2B1	6.2	53	0.57	0.16	0.61
F2C1	4.2	24	0.28	0.16	0.66
F2A2	2.7	13	0.11	0.16	0.036
F2B2	0.96	6.2	0.06	0.16	0.25
F2C2	0.54	5.3	0.05	0.16	0.24
F2A3	4.1	23	0.14	0.16	0.087
F2B3	2.2	10	0.073	0.16	0.22
F2C3	6.5	60	0.35	0.16	0.48
F3A1	11	380	3.1	0.31	1.6
F3B1	1.8	8.8	0.12	0.31	0.38
F3C1	13	870	6.7	0.31	2.1
F3A2	15	2000	9.2	0.31	1.9
F3B2	1.7	8.4	0.081	0.31	0.55
F3C2	15	2000	9.3	0.31	3.3
F3A3	13	870	3.4	0.31	1.6
F3B3	4.3	25	0.16	0.31	0.59
F3C3	9.9	240	1.24	0.31	2.0

with k_s^+ greater than 70, while F3 had 66 percent above this value. Plots of ΔU^+ versus k^+ for the three fouled specimens did not show a good collapse to the Nikuradse sand roughness function (see Fig. 5). The scaling length used in Fig. 5 was the mean biofilm height before testing. There was a high degree of scatter in these plots, although there was a significant trend of increasing ΔU^+ with increasing k^+ for all three. The mean roughness height of the biofilm measured with a paint wet film thickness gauge, by itself, does not provide an adequate roughness scaling factor. Picologlou et al. (1980) indicated a better correlation between k_s and the mean biofilm height in their pipe flow experiments. They also had difficulty in finding a functional dependency between the two, however.

Attempts to use the mean biofilm height after testing, the r.m.s. biofilm roughness, and the boundary layer thickness as scaling lengths did not lead to any better collapse of the results than the mean roughness alone. The wall datum error was also employed as a scaling length for the roughness function (Fig. 6). At higher values of ϵ^+, the slope of the roughness function is more closely aligned with the fully rough asymptote for Nikuradse sand, although there is substantial scatter in the data. The inability to adequately scale the roughness effects using a single length scale parameter is not surprising, especially for a surface as complex as a marine biofilm. Patel and Yoon (1995) note that at present there is no theoretical way to predict the roughness function based on roughness geometry alone, and a single length parameter is usually not sufficient to characterize the surface. A profile of the surface might allow a more meaningful parameter to be obtained. Since the biofilm is compliant, changes in the profile will occur with time and flow conditions. Surface topography obtained using a laser interferometer, as was used by Lee et al. (1993) on compliant surfaces, might make a more meaningful surface characterization possible. Other parameters such as the ratio of the wall shear stress to the shear modulus of the biofilm are also likely to be important.

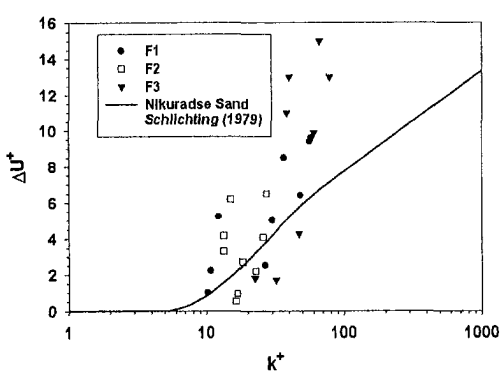

Fig. 5 Roughness functions for the fouled specimens scaled with the mean biofilm height (uncertainty in $\Delta U^+ \pm 15$ percent)

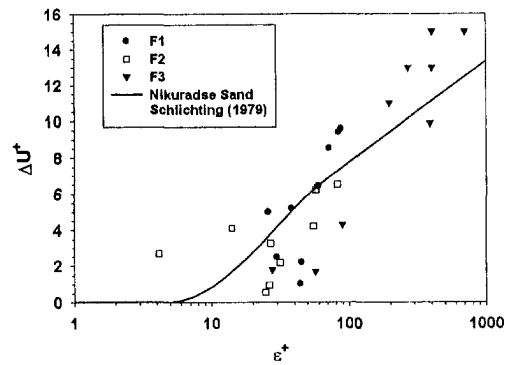

Fig. 6 Roughness functions for the fouled specimens scaled with the wall datum error (uncertainty in $\Delta U^+ \pm 15$ percent)

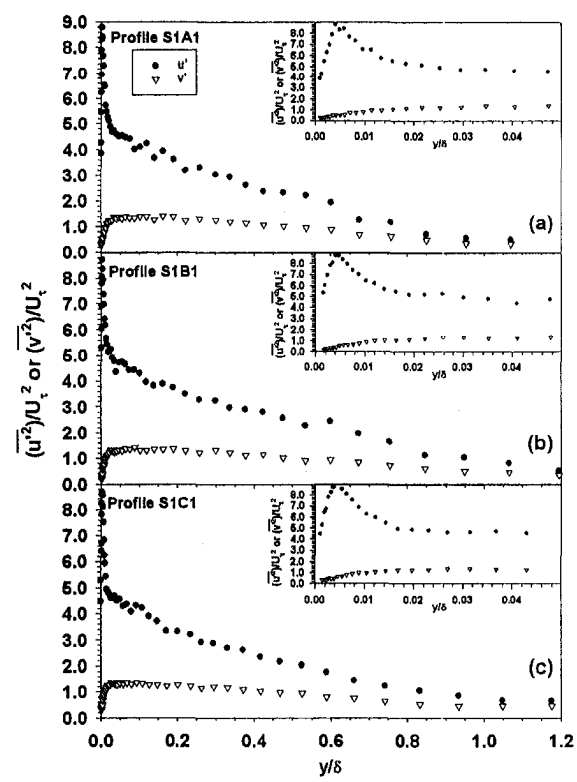

Fig. 7 Reynolds stresses $\overline{u'^2}/U_\tau^2$ and $\overline{v'^2}/U_\tau^2$ for smooth specimen, S1: (a) $x = 1.13$ m; (b) $x = 1.43$ m; (c) $x = 1.73$ m (uncertainty in $\overline{u'^2}/U_\tau^2$ and $\overline{v'^2}/U_\tau^2 \pm 6$ percent)

Downloaded 01 Apr 2008 to 131.122.81.5. Redistribution subject to ASME license or copyright; see http://www.asme.org/terms/Terms_Use.cfm

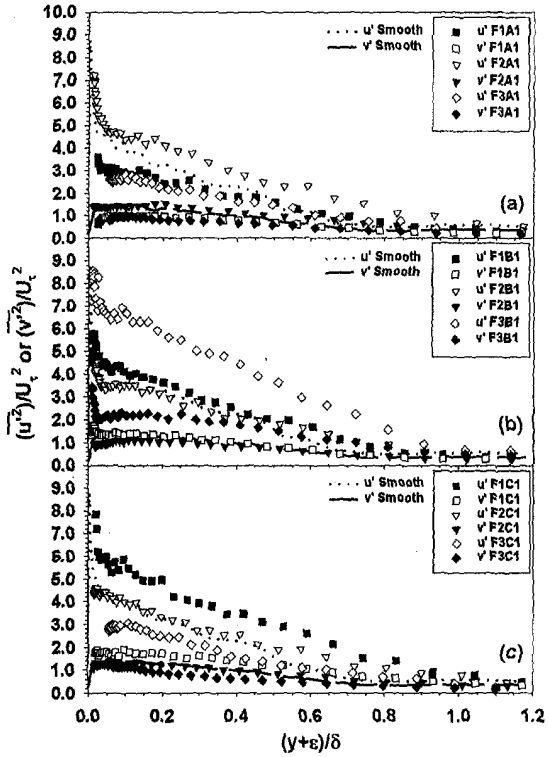

Fig. 8 Reynolds stresses $\overline{u'^2}/U_\tau^2$ and $\overline{v'^2}/U_\tau^2$ for the fouled specimens (uncertainty in $\overline{u'^2}/U_\tau^2$ and $\overline{v'^2}/U_\tau^2$ ± 15 percent)

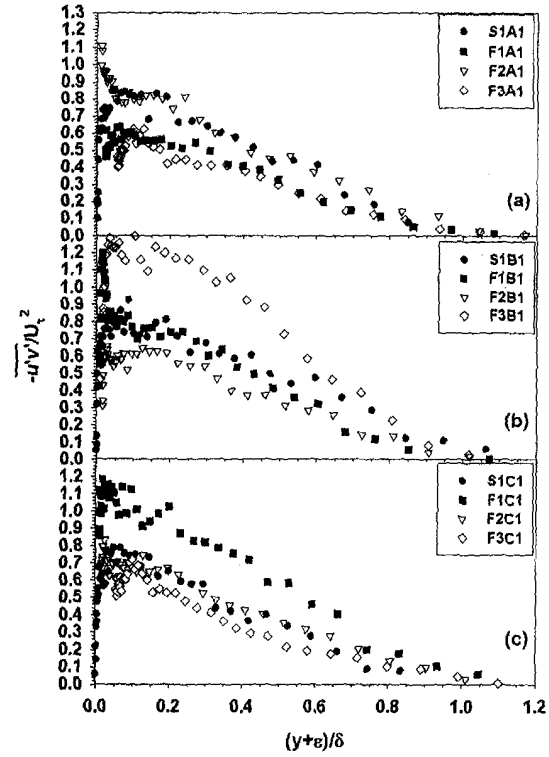

Fig. 9 Reynolds shear stress for the smooth and fouled specimens (uncertainty in normalized Reynolds stress: for smooth profiles ±8 percent; for fouled profiles ±17 percent)

The task of accurately scaling laboratory c_f's to ship scale frictional resistance coefficients (C_F) is a complex one. Even if reliable lab results for a given biofilm are available, fouling on an actual ship hull is likely to be much more heterogeneous. Differences in fouling over a hull can occur for various reasons including light shading effects, larval zonation in the water column, and differences in the flow patterns and stresses along the hull. The complexities in boundary layer flows over biofilms such as surface compliance, deformation, and removal may also increase the error in the prediction of ship scale effects. Given the inability to obtain a suitable length scale parameter to express the roughness function for these biofilms and the aforementioned difficulties, predictions of C_F at ship-scale are not offered here. It seems, however, that there is the potential for significant performance penalties as a result of low-form fouling on marine vehicles.

Normalized Reynolds stresses $\overline{u'^2}/U_\tau^2$ and $\overline{v'^2}/U_\tau^2$ for S1 and the fouled specimens are presented in Figs. 7 and 8, respectively. The profiles for S1 showed little variation with downstream distance, indicating boundary layer equilibrium. Specimen F1 showed greater streamwise variation for both $\overline{u'^2}/U_\tau^2$ and $\overline{v'^2}/U_\tau^2$. The differences observed, however, were not significant given the experimental uncertainty. Specimen F2 showed the least variation with downstream distance and collapsed to the smooth plate values within the uncertainty. Specimen F3 had the largest variation in these quantities with streamwise distance. For example, the profile for F3A1 agreed within uncertainty with the smooth results. F3B1 had significant increases in both $\overline{u'^2}/U_\tau^2$ and $\overline{v'^2}/U_\tau^2$ that extended over the entire boundary layer. F3C1 had profiles more closely resembling the smooth wall case. This rapid streamwise change in $\overline{u'^2}/U_\tau^2$ and $\overline{v'^2}/U_\tau^2$ is probably due to the patchy nature of the fouling coverage on this specimen. It seems that this variation in roughness with streamwise distance may cause production to increase or decrease in the log-law region due to the local surface condition and boundary layer history.

Krogstad and Antonia (1992) observed little change in $\overline{u'^2}/U_\tau^2$ for mesh-type roughness compared to smooth plate flows. They noted a significant increase in $\overline{v'^2}/U_\tau^2$, however. Krogstad et al. (1994) concluded that the major effect of the roughness was to tilt the large-scale structures towards the wall-normal direction, leading to a higher degree of isotropy and higher values of v'. In the present study, both $\overline{u'^2}/U_\tau^2$ and $\overline{v'^2}/U_\tau^2$ were affected to a similar degree, although there was significant variability in the profiles. Also of note were near-wall peaks in the $\overline{v'^2}/U_\tau^2$ profiles for F1B1 and F3B1 that are not seen in the smooth wall profiles. This may have resulted from local amplification of the wall-normal fluctuations due to surface compliance and movements of the algae filaments. Such features have also been observed in rough wall flows before the boundary layer reaches equilibrium (e.g., Antonia and Luxton, 1971). In the present study, the profiling stations were located between $\sim 15\delta$ to $\sim 40\delta$ from the start of the fouling. Bandyopadhyay (1987) has shown that sand roughness requires a much greater length to reach equilibrium.

Figure 9 shows the normalized Reynolds shear stress for S1 and the fouled specimens. The smooth plate profiles remained nearly constant down the plate. The F2 profiles agreed most closely with the smooth results. F2A1 did exhibit a large peak in the Reynolds shear stress in the near-wall region. The F1 profiles collapsed to the smooth plate profiles outside of the near-wall region with the exception of F1C1. In this profile, the Reynolds shear stress increased over the entire boundary layer although the uncertainty in the measurements should be noted. F1B1 showed a near-wall peak in the Reynolds shear stress was much like F2A1. Again specimen F3 exhibited the highest downstream variability. F3A1 showed lower Reynolds shear stress compared to the smooth plate, while F3B1 had a significant increase. The profiles followed trends similar to $\overline{u'^2}/U_\tau^2$ and $\overline{v'^2}/U_\tau^2$ with respect to boundary layer equilibrium. The peaked nature of some of the profiles indicate a smaller equilibrium or constant stress region than for the smooth plate flows.

Downloaded 01 Apr 2008 to 131.122.81.5. Redistribution subject to ASME license or copyright; see http://www.asme.org/terms/Terms_Use.cfm

Krogstad and Antonia (1992) noted a moderate increase in the Reynolds shear stress for rough wall flows. This was found to be due to both an increase in the magnitude of the burst and sweep events and the frequency of these events. In the present study, it is difficult to make any strong conclusions with regard to the effect of biofilms on the Reynolds shear stress due to the relatively high uncertainty in these measurements.

Conclusion

Comparisons of turbulent boundary layers over natural marine biofilms and a smooth plate have been made. The results have demonstrated the importance of low-form fouling on hydrodynamic drag. An increase in skin friction in these flows that was dependent on biofilm thickness, composition, and morphology was measured. For example, the average increase in c_f for slime films with a mean thickness of 160 μm and 350 μm was 33 and 68 percent, respectively. The average increase in c_f for a surface dominated by filamentous green algae (*Enteromorpha spp.*) with a mean thickness of 310 μm was 190 percent. Waving algae filaments seem to draw a greater amount of momentum from the mean flow than do slime films alone. A statistically significant increase in the displacement thickness (δ^*) and shape factor (H) was found for the biofilms. A standard Nikuradse sand roughness function does not sufficiently collapse the biofilm results to a universal curve using the mean roughness height as a characteristic length scale. A method of better characterizing these complex surfaces under flow may lead to a more appropriate scaling parameter. The biofilms tested showed varying effect on the Reynolds stresses normalized with U_τ.

Acknowledgments

We would like to thank the Office of Naval Research (grant #N00014-91-J-1465) and the Environmental Security and Technology Certification Program for their support of this research and their commitment to the advancement of biofouling control. Thanks go to Dr. Andrew Clark and the engineering staff at Harbor Branch Oceanographic Institution for their assistance and use of their facilities. We are also grateful to Professor Peter Bradshaw, Dr. C. S. Subramanian, and the anonymous referees for reviewing this manuscript and providing many helpful comments.

References

Acharya, M., and Escudier, M. P., 1983, "Measurements of the Wall Shear Stress in Boundary Layers," *Proceedings of the 4th International Symposium on Turbulent Shear Flows,* Karlsruhe, Germany, pp. 277–286.

Andreopoulos, J., and Wood, D. H., 1982, "The Response of a Turbulent Boundary Layer to a Short Length of Surface Roughness," *Journal of Fluid Mechanics,* Vol. 118, pp. 143–164.

Antonia, R. A., and Luxton, R. E., 1972, "The Response of a Turbulent Boundary Layer to a Step Change in Surface Roughness Part 2. Rough to Smooth," *Journal of Fluid Mechanics,* Vol. 53, Part 4, pp. 737–757.

Antonia, R. A., and Luxton, R. E., 1971, "The Response of a Turbulent Boundary Layer to a Step Change in Surface Roughness Part 1. Smooth to Rough," *Journal of Fluid Mechanics,* Vol. 48, Part 4, pp. 721–761.

Bandyopadhyay, P. R., 1987, "Rough-Wall Turbulent Boundary Layers in the Transition Regime," *Journal of Fluid Mechanics,* Vol. 180, pp. 231–266.

Benson, J. M., Ebert, J. W., and Beery, T. D., 1938, "Investigation in the NACA Tank of the Effect of Immersion in Salt Water on the Resistance of Plates Coated with Different Shipbottom Paints," NACA Memorandum Report C&R C-S19-1(3).

Bradshaw, P., 1959, "A Simple Method for Determining Turbulent Skin Friction from Velocity Profiles," *Journal of the Aeronautical Sciences,* Vol. 26, p. 841.

Coleman, H. W., and Steele, W. G., 1995, "Engineering Application of Experimental Uncertainty Analysis," *AIAA Journal,* Vol. 33, No. 10, pp. 1888–1896.

Coles, D., 1962, "The Turbulent Boundary Layer in a Compressible Fluid," The Rand Corp., Rep. R-403-PR.

Gangadharan, S., Wimberly, C. R., Clark, A., and Collino, B., 1996, "Design, Construction and Operation of a Cost Effective Water Tunnel at Harbor Branch Oceanographic Institution," Paper presented at S.N.A.M.E. Southeast Section Meeting, Oct. 11, Fort Pierce, FL.

Granville, P. S., 1987, "Three Indirect Methods for the Drag Characterization of Arbitrarily Rough Surfaces on Flat Plates," *Journal of Ship Research,* Vol. 31, No. 1, pp. 70–77.

Haslbeck, E. G., and Bohlander, G., 1992, "Microbial Biofilm Effects on Drag—Lab and Field," *Proceedings 1992 S.N.A.M.E. Ship Production Symposium.*

Klebanoff, P. S., and Diehl, F. W., 1951, "Some Features of Artificially Thickened Fully Developed Turbulent Boundary Layers with Zero Pressure Gradient," NACA TN 2475.

Krogstad, P. A., and Antonia, R. A., 1992, "Comparison Between Rough- and Smooth-Wall Turbulent Boundary Layers," *Journal of Fluid Mechanics,* Vol. 245, pp. 599–617.

Krogstad, P. A., Antonia, R. A., and Browne, L. W. B., 1994, "Structure of Turbulent Boundary Layers on Smooth and Rough Walls," *Journal of Fluid Mechanics,* Vol. 277, pp. 1–21.

Lee, T., Fisher, M., and Schwarz, W. H., 1993, "Investigation of the Stable Interaction of a Passive Compliant Surface with a Turbulent Boundary Layer," *Journal of Fluid Mechanics,* Vol. 257, pp. 373–401.

Lewkowicz, A. K., and Das, D. K., 1981, "Turbulent Boundary Layers on Rough Surfaces With and Without a Pliable Overlayer: A Simulation of Marine Fouling," *Proceedings of the A.S.M.E/A.S.C.E. Bioengineering, Fluid Engineering, and Applied Mechanics Conference,* pp. 174–186.

Lewthwaite, J. C., Molland, A. F., and Thomas, K. W., 1985, "An Investigation into the Variation of Ship Skin Frictional Resistance with Fouling," *Transactions Royal Institute of Naval Architects,* Vol. 127, pp. 269–284.

Ligrani, P. M., and Moffat, R. J., 1986, "Structure of Transitionally Rough and Fully Rough Turbulent Boundary Layers," *Journal of Fluid Mechanics,* Vol. 162, pp. 69–98.

Loeb, G. I., Laster, D., and Gracik, T., 1984, "The Influence of Microbial Fouling Films on Hydrodynamic Drag of Rotating Discs," *Marine Biodeterioration, An Interdisciplinary Study,* J. D. Costlow and R. Tipper, eds., Naval Institute Press, Annapolis, MD, pp. 88–94.

Marine Fouling and Its Prevention, U.S. Naval Institute Press, Annapolis, MD, 1952.

McEntee, W., 1915, "Variation of Frictional Resistance of Ships with Condition of Wetted Surface," *Transactions Society of Naval Architects and Marine Engineers,* Vol. 24, pp. 37–42.

Patel, V. C., and Yoon, J. Y., 1995, "Application of Turbulence Models to Separated Flow over Rough Surfaces," ASME JOURNAL OF FLUIDS ENGINEERING, Vol. 117, June, pp. 234–241.

Perry, A. E., and Joubert, P. N., 1963, "Rough-Wall Turbulent Boundary Layers," *Journal of Fluid Mechanics,* Vol. 37, pp. 383–413.

Perry, A. E., Schofield, W. H., and Joubert, P. N., 1969, "Rough Wall Turbulent Boundary Layers," *Journal of Fluid Mechanics,* Vol. 37, Part 2, pp. 383–413.

Picologlou, B. F., Zelver, N., and Characklis, W. G., 1980, "Biofilm Growth and Hydraulic Performance," ASCE *Journal of the Hydraulics Division,* HY5, pp. 733–746.

Schlichting, H., 1979, *Boundary-Layer Theory,* Seventh Edition, McGraw-Hill.

Schultz, M. P., 1998, "The Effect of Biofilms on Turbulent Boundary Layer Structure," Florida Institute of Technology, Ph.D. Dissertation, May.

Sokal, R. R., and Rohfl, F. J. Biometry, 1981, *The Principles and Practice of Statistics in Biological Research,* W. H. Freeman, San Francisco.

Thole, K. A., and Bogard, D. G., 1996, "High Freestream Turbulence Effect on Turbulent Boundary Layers," ASME JOURNAL OF FLUIDS ENGINEERING, Vol. 118, pp. 276–284.

Winter, K. G., 1977, "An Outline of the Techniques Available for the Measurement of Skin Friction in Turbulent Boundary Layers," *Progress in the Aerospace Sciences,* Vol. 18, pp. 1–57.

Downloaded 01 Apr 2008 to 131.122.81.5. Redistribution subject to ASME license or copyright; see http://www.asme.org/terms/Terms_Use.cfm